Key Engineering Materials
ISSN: 1662-9795, Vol. 1051, pp 135-146
doi:10.4028/p-4eKwco

Submitted: 2026-01-19
Revised: 2026-02-12
Accepted: 2026-02-17
Online: 2026-04-17

Comparing Different Sheet Metal Forming Processes for Reshaping Purposes

PICCININNI Antonio[1,a*], INGARAO Giuseppe[2,b], BARCELLONA Letizia[1,c], PULEO Riccardo[2,d], CUSANNO Angela[1,e], MICARI Fabrizio[2,f] and PALUMBO Gianfranco[1,g]

[1]Department of Mechanics, Mathematics and Management - Politecnico di Bari, via Orabona, 4 Bari 70126, Italy

[2]Department of Engineering, University of Palermo, Viale delle Scienze, Palermo 90128, Italy

[a]antonio.piccininni@poliba.it, [b]giuseppe.ingarao@unipa.it, [c]l.barcellona@phd.poliba.it, [d]riccardo.puleo01@unipa.it, [e]angela.cusanno@poliba.it, [f]fabrizio.micari@unipa.it, [g]gianfranco.palumbo@poliba.it

Keywords: Gas forming, Hydroforming, SPIF, Reshaping, EoL, Sustainability

Abstract. The reshaping approach is widely considered a virtuous strategy in line with the pillars of the Circular Economy. According to this approach, End-of-Life (EoL) components are subjected to a second forming process to achieve a new functional geometry. However, EoL parts often exhibit a non-uniform thickness distribution and work-hardened zones resulting from the primary manufacturing step, which makes the design of the reshaping step not trivial. Beyond the standard objectives like avoiding fracture and minimizing springback during the reshaping operations, one of the most concerning aspects is the complete removal of the geometrical features coming from the initial forming process.

Flexibility and versatility of the forming process are unavoidable requirements to make the reshaping successful. Therefore, three different reshaping routes are numerically investigated in the present work: (i) reshaping by hydroforming (RH) at room temperature; (ii) reshaping by gas forming (RGF) at hot temperature; (iii) a hybrid approach, based on the combination of an intermediate deformation step via Single Point Incremental Forming followed by sheet hydroforming (RHA). The three routes share the same EoL, characterized by the presence of a deep-drawn square feature. Comparing the three routes, in terms of final shape and thinning distribution, with a reference case study (represented by the sole hydroforming process carried out on an undeformed flat blank) allowed to conclude that the feature removal and a non-severe thinning could not be achieved simultaneously: in fact, while RGF and RHA ensure a more evident suppression of the pre-existing feature, they simultaneously induce a more pronounced and localized thinning compared to the RH route.

Introduction

The reduction of the environmental impact associated with industrial production has become a key priority, particularly in sectors characterized by high energy consumption and greenhouse gas emissions. Among structural materials, aluminium plays a critical role: despite its favorable strength-to-weight ratio and recyclability, primary aluminium production remains one of the most energy and emission-intensive industrial processes [1]. As global demand for aluminium products continues to grow [2], the adoption of effective circular economy strategies is essential to decouple resource consumption from economic development. In this context, conventional recycling routes based on remelting, although widely adopted, present visible limitations. In addition to the high energy demand, remelting processes are affected by permanent material losses due to oxidation, particularly for aluminium alloys. For these reasons, increasing attention has been given to alternative approaches capable of preserving both material integrity and manufacturing value. Solid-state recycling [3,4] and direct reuse strategies have therefore emerged as promising solutions to further reduce the environmental footprint of metal products. Within the metal reuse category, reshaping has demonstrated particular attractiveness. This approach consists of applying manufacturing techniques

(additive, subtractive, or mass-conserving) to rework End-of-Life (EoL) components by modifying their shape. In this way, reshaping enables the recovery not only of the material but also of the geometric and functional value embedded in the component. However, reshaping poses significant technological challenges, especially when sheet metal components are considered. EoL sheet parts typically exhibit heterogeneous thickness distributions, localized strain hardening, and reduced residual formability as a result of their original manufacturing history. These aspects make the design of reshaping processes substantially more complex than that of conventional forming operations starting from undeformed flat sheets. Despite its potential, the reshaping of sheet metal components has received limited attention in the literature so far. Existing studies mainly focus on flexible forming technologies, such as Single Point Incremental Forming or Hydroforming, due to their ability to accommodate complex strain paths and non-uniform material conditions.

In particular, Single Point Incremental Forming (SPIF) is a flexible sheet metal forming process based on localized and progressive deformation induced by a hemispherical tool following a digitally defined toolpath, without the need for dedicated dies. Compared to conventional stamping processes, it enables higher formability due to the localized low forming forces involved and the delayed onset of fracture, making it possible to impart additional deformation even in regions that have already undergone significant straining. Previous studies have demonstrated the feasibility of SPIF-based reshaping by applying the process to deep-drawn components into new geometries, while preserving material integrity [3]. Takano et al. [5] applied Single Point Incremental Forming (SPIF) to reform a pre-bent sheet. From a sustainability perspective, SPIF-based reshaping represents an effective alternative to conventional recycling routes, as it reduces the number of process steps [6], minimizes material losses, and leads to significant reductions in energy consumption and CO_2-equivalent emissions.

On the contrary, Sheet Hydroforming (SHF) is a sheet metal forming technology that exploits fluid pressure to shape metallic blanks, enabling the production of complex geometries with high dimensional accuracy. This technique can operate with a single rigid die, as the forming load is uniformly applied by the pressurized fluid, resulting in reduced tooling requirements and process complexity [4], and making SHF particularly suitable for reshaping applications, where additional deformation must be imposed on preformed or EoL components without inducing premature failure. Moreover, it offers several advantages over other sheet metal forming technologies [7], including enhanced formability limits [8], the capability to produce more complex geometries such as re-entrant features [9], and, in some cases, a reduced number of forming steps [6]. For example, Brosius et al. [10] operated a SHF process to reshape an engine hood into a rectangular sheet. However, residual marks may remain in less-deformed regions when the strain imposed is insufficient [5].

In previous works, the feasibility of reshaping deep-drawn aluminium components by means of SHF was experimentally and numerically demonstrated. Those studies highlighted that, while SHF can effectively produce a new geometry to EoL components, the complete removal of pre-existing features is strongly dependent on the local deformation conditions experienced during the reshaping step. In particular, residual marks from the original deep-drawn geometry were observed when the imposed strain during hydroforming was insufficient, whereas excessive restraining conditions led to premature fracture. These findings clearly indicate that the reshaping process design requires the introduction of additional objectives and constraints compared to conventional sheet metal forming.

Based on this background, the present work investigates the performance of remodeling based on different approaches: literature-tapped SHF, gas forming (GF), and SHF with the introduction of an intermediate SPIF phase. The Gas Forming, particularly in its hot variant, was selected due to its potential advantages over conventional forming and SHF in the reshaping of end-of-life (EoL) sheet metal components. The gradual and uniform pressure application, offered by this technique, promotes a more homogeneous strain redistribution, which is beneficial for mitigating residual geometric features and handling the heterogeneous thickness distributions and limited residual formability typical of EoL parts [11]. The intermediate SPIF step was, instead, intended to promote smoother transformation of the deep-drawn feature geometry, before the final hydroforming stage, aiming to facilitate the feature removal during the hydroforming process. The feasibility of both routes was

assessed through finite element simulations in the Abaqus environment, focusing on the influence of key process parameters on the reshaped component. A deep drawn square feature was used to represent the EoL geometry [12], and the variations of the descending angle for SPIF were considered. All parameters were tested along two deformation directions, corresponding to the top and bottom of the EoL feature. The resulting performance was compared in terms of sheet thinning and feature removal capability.

Materials and Methods.

Investigated reshaping routes. This work expands the research through a comparative numerical investigation of three different technological routes. The three strategies, more detailed in the following, share the same EoL represented by a sheet metal-based part characterized by the presence of a square-based feature obtained from a previous Deep Drawing process (Fig. 1a), whose geometry is defined according to [12] (Fig. 2a). The Deep Drawing-derived feature was selected because it represents a critical condition in terms of strain hardening, as it promotes highly localized plastic deformation. In particular, the selected EoL component is characterized by concentrated strain levels at the bottom corner of the deep-drawn feature, whereas lower strain levels are observed in other regions. Consequently, the part effectively mimics a realistic EoL component, showing a heterogeneous distribution of both strain hardening and thickness, carrying its own deformation history and thickness heterogeneity, thus serving as a suitable benchmark for assessing the capabilities of the reshaping approach [13].

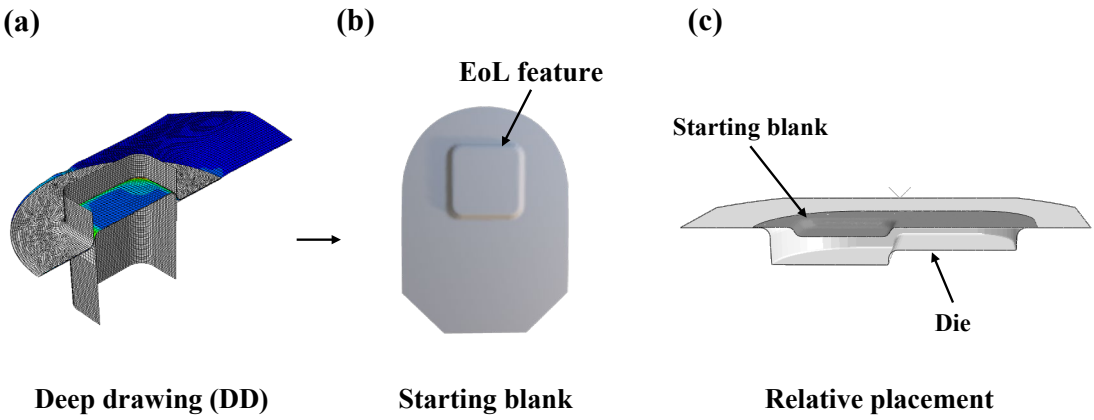

Fig. 1. Illustration of the (a) pre-feature of the EoL component obtained through DD, (b) starting blank with the deformation history, (c) section views of the blank and die positioning

The final reshaped part is defined by the geometry of the die depicted in Fig. 2b [12]. It is worth mentioning that the geometry of the die cavity is not related to any specific industrial component, but it is more regarded as a benchmark geometry: the two-steps induces two different levels of strain, and the 5 mm fillet between the two imparts a condition close to the plane strain. The geometry, thus, allows for challenging the capabilities of the reshaping approach to different extents across different states of deformation. Another common aspect of the three strategies concerns the positioning of the deep-drawn feature during the reshaping step: specifically, it was oriented with its concavity aligned with the deepest step of the die cavity. Moreover, the EoL component was positioned so that the wall of the deep-drawn feature was aligned with a vertical die wall near the fillet between the two depth levels (Fig. 1c).

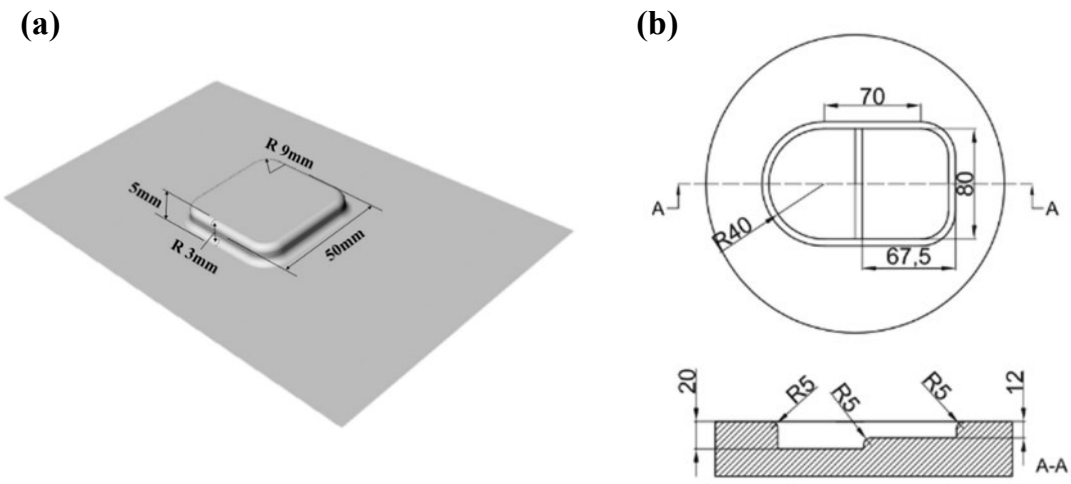

Fig. 2. Illustration of (a) Deep-Drawing feature dimensions and (b) geometry of the die cavity

To ensure the effectiveness of each approach, the performance of the three strategies was evaluated against the shape reference condition (indicated as SR) and defined as the geometry obtained by hydroforming when starting from an initial undeformed blank. The three strategies are detailed in the following.

1. Reshaping by Hydroforming (*RH*): the EoL component is reshaped considering a deformation step of hydroforming at room temperature, according to the approach detailed in [12].
2. Reshaping by Gas Forming (*RGF*): the reshaping of deep-drawn EoL [14] is carried out considering the deformation by a pressurized gas at high temperature (higher than half of the material's melting temperature).
3. Reshaping by Hybrid Approach (*RHA*): an original methodology is proposed, involving an intermediate Single Point Incremental Forming (SPIF) stage followed by hydroforming. The SPIF step is intended to induce localized, progressive deformation to "prepare" the geometry, facilitating the subsequent removal of residual features during the subsequent hydroforming step.

The entire investigation is conducted exclusively within a numerical framework using the Abaqus finite element code. The analysis of the numerical results was carried out by looking at the post-forming properties of the reshaped part (final shape and final thickness distribution) and comparing them with those from the reference SR case.

Reshaping by hydroforming - RH. The FE model used to simulate the HF process is detailed in [12], and it is here briefly recalled. The reshaping step was simulated sequentially after the deep drawing step, detailed in the previous section, within the same numerical model. The AA5754-H22 blanks were modelled as a deformable shell body with an initial thickness of 0.5 mm. The hydroforming die, on the other hand, was modelled as a shell rigid body. Contact between the bodies was governed by setting a friction coefficient of 0.125 [15]. The material behavior was implemented in the finite element (FE) model by integrating the flow stress curve, derived from uniaxial tensile tests performed on dog bone samples according to UNI EN ISO 6892, together with the forming limit curve (FLC) [13]. The main process parameters, linearly increased during the forming step, are listed in Table 1.

Table 1. Reshaping by hydroforming (RH): process parameters

Time [s]	Holder force [N]	Oil [MPa]
0	0	0
1	16500	0
53	28500	5.2

The hydroforming was simulated using the Abaqus/Explicit solver. To reduce the computational efficiency, the symmetry of the system was exploited by modeling only half of the domain (Fig. 3). A semi-automatic mass scaling approach was adopted, and the stable time increment was carefully selected to ensure that the system's kinetic energy remained negligible with respect to the internal energy.

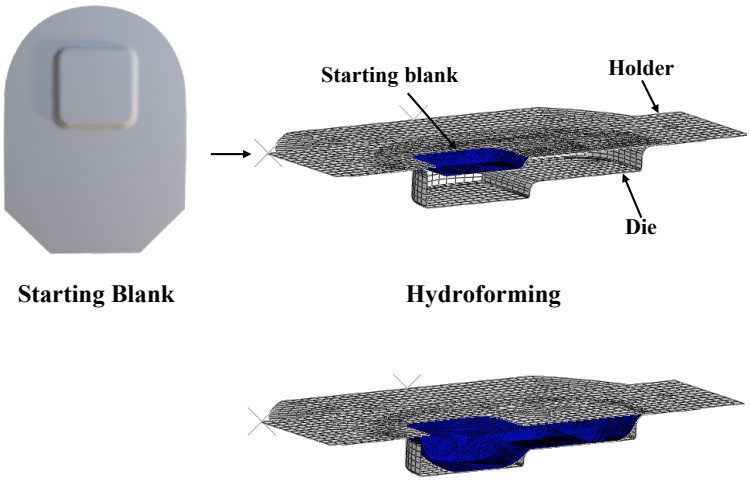

Fig. 3. FE model of the HF process

Reshaping by gas forming - RGF. For the simulation of the RGF approach, the blank deformed after the DD step was exported and reimported into the numerical model of the gas forming step, along with the final thickness distribution. On the other hand, the heterogeneous distribution of the work-hardening was not imported as an initial condition since the exposure of the blank to 400 °C was considered sufficient to anneal the heterogeneity of work-hardening distribution, as well as the residual state of stress [14].

The material behavior was modelled according to the Backofen law (Eq. 1) that correlates the equivalent state of stress with the equivalent strain rate by means of the two constants (the strength coefficient C and the strain rate sensitivity exponent m).

$$\sigma = C \cdot \dot{\varepsilon}^{m} \tag{1}$$

The two constants were inversely determined from an extensive experimental characterization based on a free inflation test on 0.5 mm thick samples and carried out at 400 °C.

The preliminary experimental tests also allowed to identify the strain rate of 0.002 s^{-1} as the optimal condition to enhance the material formability.

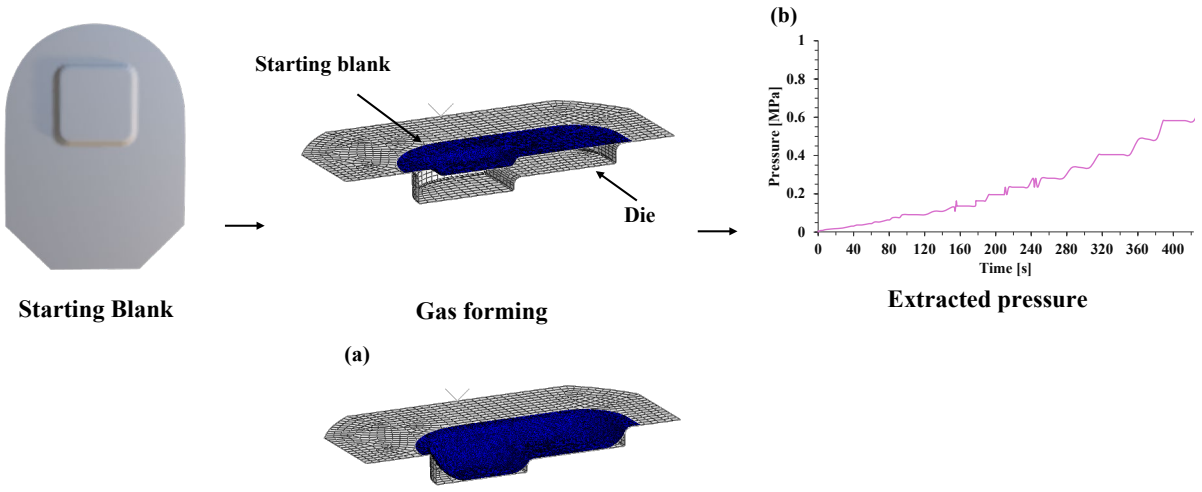

Fig. 4. (a) FE model of the GF process, (b) pressure profile for keeping the strain rate close to the optimal

The modelled assembly is reported in Fig. 4 and shows some analogies with the hydroforming model. The blank is again modelled as a 3D deformable body, while keeping the rigid formulation for the die. The blank, unlike the HF process, is completely constrained at its border in order to prevent any material draw-in according to the actual conditions of the real process. From the numerical point of view, one of the biggest advantages of the numerical approach is the possibility to calculate the gas pressure profile as an output (differently from what happens for the hydroforming process, where the operator defines the oil pressure variation as an input, as also shown in Table 1). In this specific case, the optimal strain rate identified during the material characterization was imposed as a target in the numerical simulation: thanks to the availability of an internal routine, the Abaqus solver was able to calculate the gas pressure curve (an example is shown in Fig. 4b) while keeping the overall strain rate close to the target value. In order to keep the consistency in the comparison of the reshaping strategies, the post-reshaping properties from the RGF approach were extracted at the time frame when the blank shape profile (measured along the longitudinal plane of symmetry) was close to the one from the reference SR case.

Reshaping by hybrid approach - RHA. The third investigated route, RHA, involves an intermediate Single Point Incremental Forming (SPIF) aimed at reducing the geometric impact of the EoL feature and promoting a smoother removal during the subsequent hydroforming step. In accordance with the RH approach, the material behavior alloy was modelled using the flow curve and the forming limit curve.

The SPIF process was modeled using a dynamic-explicit simulation subdivided into two main steps: the clamping of the blank and the incremental forming operation. Since the tool moved along a predefined trajectory, no symmetry could be exploited, and the whole system was thus modelled. For the sake of clarity, a view cut of the single steps using the longitudinal symmetry plane is reported in Fig. 5.

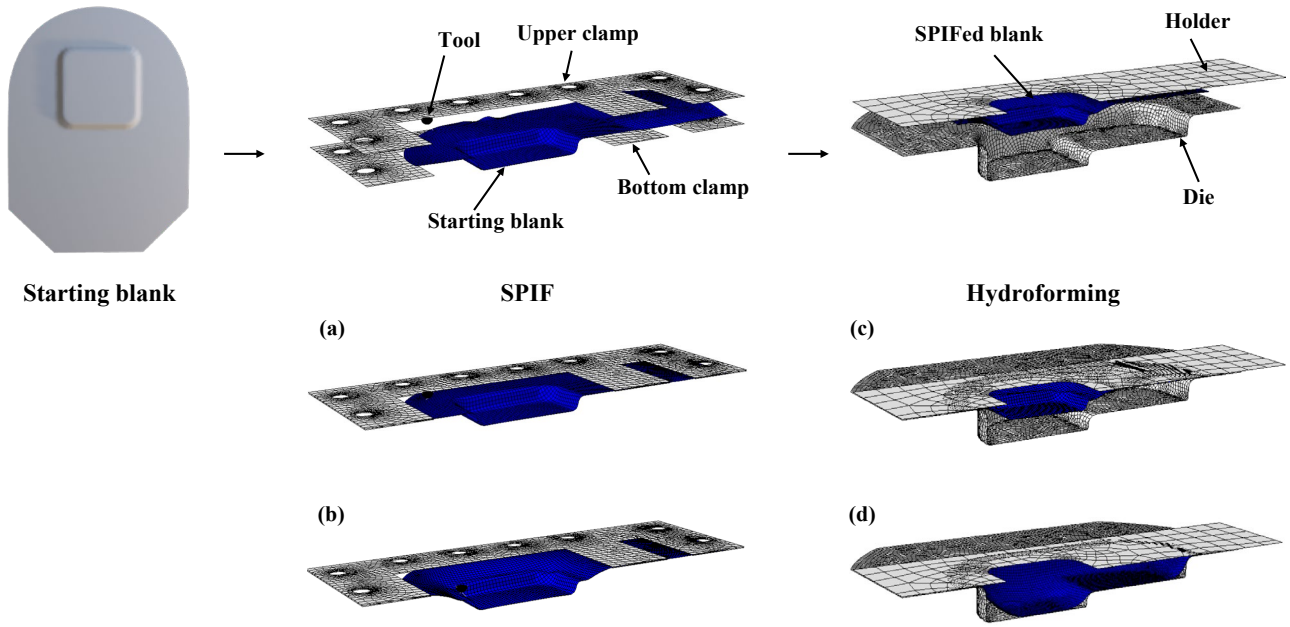

Fig. 5. Description of the SPIF and HF phases: (a) clamping of the blank, (b) SPIF process, (c) clamping of the SPIFed sample, and (d) HF process

This process was modelled through a dynamic-explicit simulation, including a specifically designed clamping system. The intermediate phase was structured into two steps: clamping of the sheet (Fig. 5a) and deformation by SPIF (Fig. 5b). All the components of the clamping system, as well as the tool, were considered rigid bodies, whereas the blank was defined using the state variables imported from the previous deep drawing step. The lubrication condition at the tool-blank interface was modelled using a Coulomb friction coefficient of 0.05, consistent with values reported in the literature [16], whereas the tool motion in three-dimensional space was implemented by imposing a displacement profile along the x-, y-, and z-directions, calculated in MATLAB. The intermediate

SPIF step was simulated according to different loading conditions characterized by three values of the descending angle (α), namely 30°, 40°, and 50° (Fig. 6b) along a pyramidal toolpath. For the sake of simplicity, the following nomenclature will be adopted: RHA30, RHA40, and RHA50 for the angles 30°, 40°, and 50°, respectively.

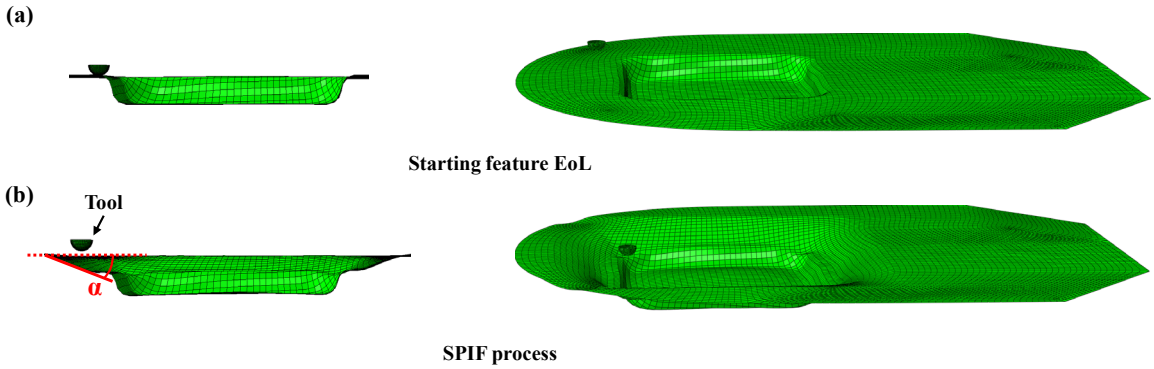

Fig. 6. Refiguration of the (a) starting blank with the feature, (b) descending angle (α) in the SPIF process

After each forming stage, from deep drawing (DD) to hydroforming (HF), a springback analysis was performed in order to account for the residual stress state induced by the preceding operations. Also in this case, the HF process was subdivided into a clamping step (Fig. 5c) and a hydroforming step (Fig. 5d), where the blank holder closing force and the applied oil pressure were modelled as in the case of the RH (see Table 1).

Result and Discussion

The performance of the proposed approaches has been evaluated by comparing the final thickness distribution and the effectiveness in removing the deep-drawn feature against the reference SR case (hydroformed step starting from an undeformed flat blank). Moreover, the analysis was carried out at two different levels: initially, the three intermediate SPIF strategies were compared by looking at the blank shape and the thickness distribution along the longitudinal symmetry plane (0°) and along a 45° section (corresponding to the diagonal of the EoL deep-drawn feature); always considering the same two planes, the final reshaped geometries from the three described strategies were also compared (in Fig. 7 an example is given for the sake of clarity).

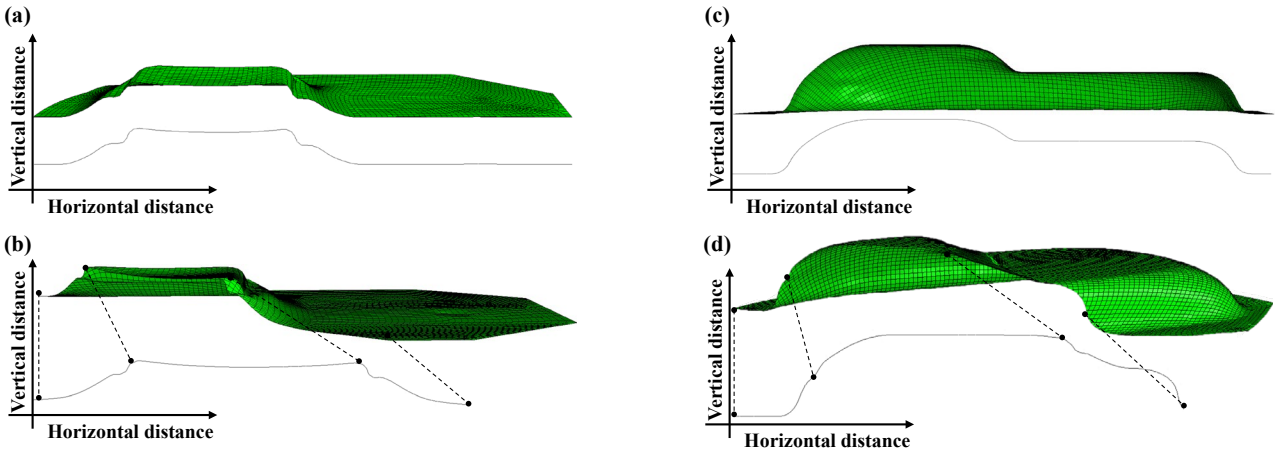

Fig.7. Visualization of the sections used for process comparison. (a) longitudinal and (b) 45° section of the part after the SPIF process; (c) longitudinal and (d) 45° section of the part obtained after the reshaping processes, along with the contour profile (grey line)

The intermediate SPIF step has been successfully simulated, and the results are depicted in Fig. 8a and Fig. 8b for the 0° and 45° sections, respectively. In these figures, the deformed profile (continuous lines) and the thickness (dotted lines) are plotted together. It emerges that the smoothest surface condition was achieved by RHA50, albeit at the expense of thickness. In fact, as is visible in the 45° section, the minimum thickness values of approximately 0.36 and 0.38 mm were observed near the edge of the EoL feature, corresponding to the region most affected by the tool action. This represents a thickness reduction of about 28% and 24%. For the other two configurations, the presence of the EoL feature remains evident in Figure 8, as a distinct step is still observed at 4 and 6 mm (Fig. 8a) for RHA30 and RHA40, respectively, but the thickness reduction remains limited to 14% and 6%.

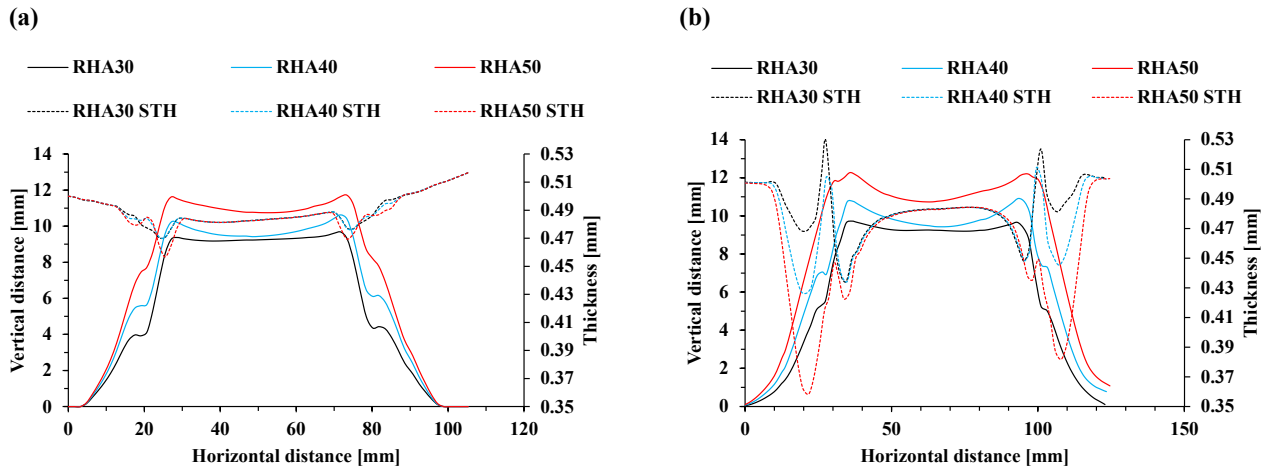

Fig. 8. Deformed profile (continuous) and thickness distribution (dot) of (a) longitudinal and (b) 45° section, for RHA30, RHA40, and RHA50

The deformed shapes for all investigated cases are shown below. From this comparison, it is possible to identify the RHA configuration that achieves the most effective removal of the EoL feature, which corresponds to the strategy RHA50 (Fig. 9d). Consequently, only this specific case is retained for the subsequent detailed analyses.

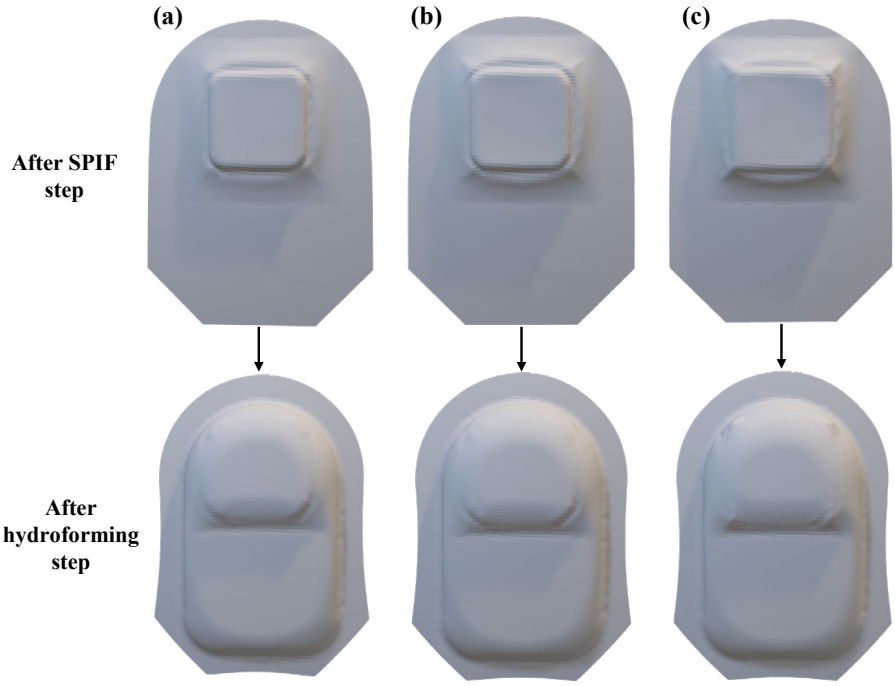

Fig. 9. Comparison among the three RHA approaches: (a) RHA30, (b) RHA40, and (c) RHA50

The results illustrated in Fig. 10 allow us to compare the effectiveness of remodeling strategies along two critical sections, analyzing both the recovery of the geometric shape (Fig. 10a, b) and the distribution of thicknesses (Fig. 10c, d). The SR is represented by the green curve, which indicates the formation of a flat blank without EoL defects, as presented previously.

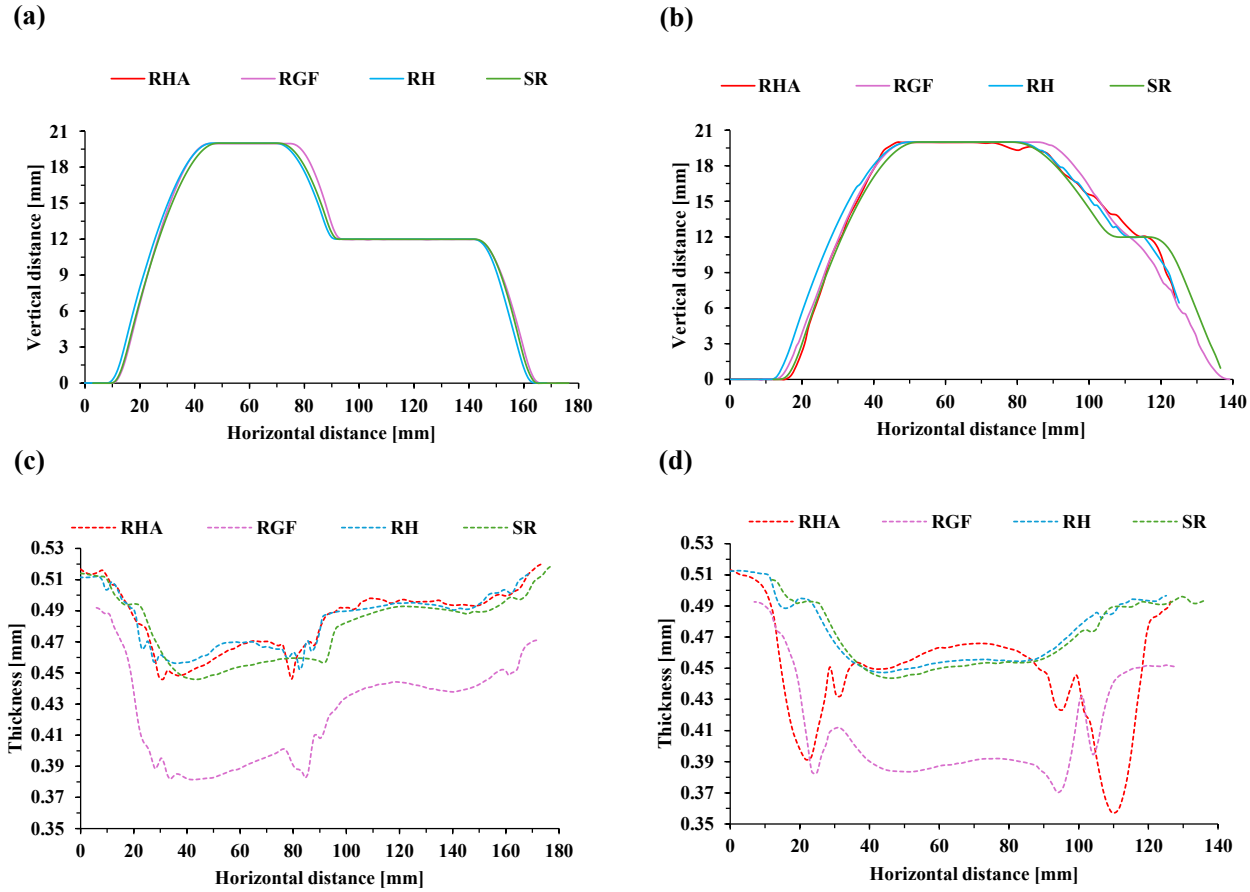

Fig. 10. Results of: (a) deformed profile in the longitudinal section, (b) deformed profile in the 45° section, (c) thickness distribution in the longitudinal section, (d) thickness distribution in the 45° section

The observation of the final shape along the 0° plane (Figure 10 a) does not allow for fully capturing the effectiveness of the process in removing the feature, since the geometric discrepancies between the cases are limited. However, extremely interesting results emerge from the thickness analysis (Figure 10c). The SR (green curve) shows thickness values not far from the RHA and RH approaches. In these cases, the presence of the pre-existing feature combined with the material draw-in during the hydroforming led to a less severe thinning than in the SR case.

Specifically, along the highlighted plane, low thinning is shown, with values around 0.45 mm (reduction of approximately 10%). In contrast, the GF process already shows more marked thinning levels, reaching approximately 0.38 mm (24% reduction) at the edges of the feature, which is expected due to the type of deformation induced during the process.

Section along the 45° direction (Fig. 10b, d) is crucial for evaluating the surface quality and the extent of the contact between the blank and the die wall. In the reference condition (SR), the step is clearly visible and represents the correct contact of the material with the wall. A similar profile, although very jagged, is observed in the RHA and RH cases, a phenomenon justified by the sliding of the material towards the deepest step area of the die.

The RH approach (blue curve) exhibits slight limitations in removing the EoL feature; specifically, between 100 and 120 mm of horizontal distance, the profile shows reduced smoothness. This smoothness improves with the addition of RHA50 (red curve). In this case, however, the minimum thickness drops sharply to 0.36 mm, corresponding to a 28% reduction. RGF stands out clearly: by not allowing the material to draw in due to the constraint conditions, the process operates by pure

stretching (Fig. 10b, purple curve). As a consequence, the contact between the blank and the die wall is not as evident as in the other strategies (where the material draw-in helps in this regard). The analysis of the thinning distribution along the 45° direction reveals significantly different profiles across the investigated strategies. While RH shows a thickness distribution comparable to the SR case, the RGF process clearly presents the most unfavorable conditions in terms of average thickness.

In contrast, the RHA approach, although more effective than RH for geometric recovery, shows the most marked localized thinning and the highest degree of inhomogeneity. In this case, although the central zone keeps values around 0.45 mm, sharp drops in thickness are observed in the transition zones. Specifically, the thickness reaches minimum values of approximately 0.35 mm near the second step of the die (at a horizontal distance of 110 mm, red curve). This localized thinning is the result of the strain accumulated by the preliminary SPIF phase, followed by the final hydroforming pressure. Fig. 11 shows an overall comparison of the three investigated reshaping strategies against the reference condition.

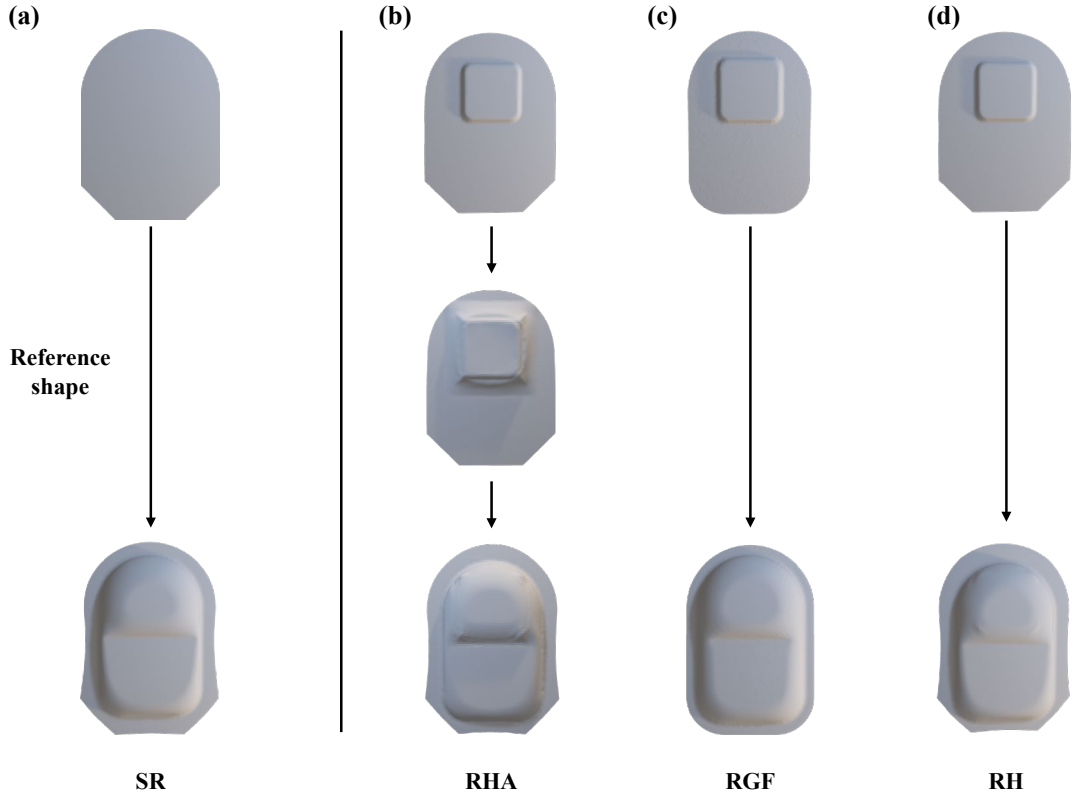

Fig. 11. Overall comparison among the reshaping strategies investigated

Conclusions.

In this work, three distinct reshaping alternatives - Reshaping by hydroforming (RH), Reshaping by gas forming (RGF), and the Reshaping by hybrid approach (RHA) - were numerically applied to an AA5754-H22 End-of-Life (EoL) component to investigate their feasibility in removing residual geometric features. Based on the numerical results, the following conclusions can be drawn:

- The research provided a rigorous comparison between RH, RHA, and RGF, benchmarking their performance against the Shape Reference (SR). While the longitudinal plane (0°) did not show a clear distinction in feature removal capability, the thickness analysis revealed that the pre-existing EoL feature at the die bottom facilitates the new deformation, limiting thinning for cold processes to approximately 10% compared to the SR case.
- RH showed low capability in removing the EoL feature, leaving a geometric step in the 45° section between 100 and 120 mm of horizontal distance. However, this process ensured a thickness distribution very close to the SR target.

- The intermediate SPIF phase in the RHA route demonstrated a significant ability to modify the EoL geometry, with surface smoothness improving as the descending angle (α) increased to 50°. The material flow associated with this improvement resulted in a more jagged profile and severe localized thinning, reaching approximately 0.36 mm (a 28% reduction) in the 45° section.
- RGF ensured more effective feature suppression compared to the other routes: by operating primarily through stretching due to the absence of material draw-in, RGF recorded the most critical thinning levels, with minimum values of 0.35 mm (30%) and 0.38 mm (24%) in the 45° and longitudinal sections, respectively.
- It is worth mentioning that a unique thinning threshold cannot be defined, as allowable thinning levels strongly depend on the intended second-life application and the functional requirements of the reshaped component. The investigated case study was more focussed on demonstrating the effectiveness of the reshaping approach when the starting EoL part is characterized by a pronounced heterogeneity in its properties (strain and work-hardening distribution).

Further experimental campaigns will be conducted to validate the numerical results of the different approaches. Moreover, newly optimized tool paths will be investigated to improve feature removal and to mitigate the thinning phenomenon in the intermediate SPIF process.

Acknowledgement

This work was carried out within the framework of the project "Going Beyond Recycling: Reshaping of End-of-Life Components through Advanced Sheet Metal Forming Processes", funded under the PRIN 2022 Call (MUR Decree No. 1401 of 18/09/2024 - CUP I53C24002500006).

References

[1] Cusano G. Best Available Techniques (BAT) Reference Document for Waste Incineration. 2019.

[2] Raabe D, Ponge D, Uggowitzer PJ, Roscher M, Paolantonio M, Liu C, et al. Making sustainable aluminum by recycling scrap: The science of "dirty" alloys. Prog Mater Sci 2022;128. https://doi.org/10.1016/j.pmatsci.2022.100947.

[3] Wan B, Chen W, Lu T, Liu F, Jiang Z, Mao M. Review of solid state recycling of aluminum chips. Resour Conserv Recycl 2017;125:37–47. https://doi.org/10.1016/j.resconrec. 2017.06.004.

[4] Duflou JR, Tekkaya AE, Haase M, Welo T, Vanmeensel K, Kellens K, et al. Environmental assessment of solid state recycling routes for aluminium alloys: Can solid state processes significantly reduce the environmental impact of aluminium recycling? CIRP Ann Manuf Technol 2015;64:37–40. https://doi.org/10.1016/j.cirp.2015.04.051.

[5] Takano H, Kitazawa K, Goto T. Incremental forming of nonuniform sheet metal: Possibility of cold recycling process of sheet metal waste. Int J Mach Tools Manuf 2008;48:477–82. https://doi.org/10.1016/j.ijmachtools.2007.10.009.

[6] Sato H, Manabe K, Ito K, Wei D, Jiang Z. Development of servo-type micro-hydromechanical deep-drawing apparatus and micro deep-drawing experiments of circular cups. J Mater Process Technol 2015;224:233–9. https://doi.org/10.1016/j.jmatprotec.2015.05.014.

[7] Bell C, Corney J, Zuelli N, Savings D. A state of the art review of hydroforming technology: Its applications, research areas, history, and future in manufacturing. International Journal of Material Forming 2020;13:789–828. https://doi.org/10.1007/s12289-019-01507-1.

[8] Lang LH, Wang ZR, Kang DC, Yuan SJ, Zhang SH, Danckert J, et al. Hydroforming highlights: sheet hydroforming and tube hydroforming. J Mater Process Technol 2004;151:165–77. https://doi.org/10.1016/j.jmatprotec.2004.04.032.

[9] Parsa MH, Darbandi P. Experimental and numerical analyses of sheet hydroforming process for production of an automobile body part. J Mater Process Technol 2008;198:381–90. https://doi.org/https://doi.org/10.1016/j.jmatprotec.2007.07.023.

[10] Brosius A, Hermes M, Khalifa N Ben, Trompeter M, Tekkaya AE. Innovation by forming technology: motivation for research. International Journal of Material Forming 2009;2:29–38.

[11] Duflou JR, Tekkaya AE, Haase M, Welo T, Vanmeensel K, Kellens K, et al. Environmental assessment of solid state recycling routes for aluminium alloys: Can solid state processes significantly reduce the environmental impact of aluminium recycling? CIRP Annals 2015;64:37–40. https://doi.org/https://doi.org/10.1016/j.cirp.2015.04.051.

[12] Piccininni A, Cusanno A, Palumbo G, Zaheer O, Ingarao G, Fratini L. Reshaping End-of-Life components by sheet hydroforming: An experimental and numerical analysis. J Mater Process Technol 2022;306:117650. https://doi.org/10.1016/j.jmatprotec.2022.117650.

[13] Ingarao G, Zaheer O, Campanella D, Fratini L. Re-forming end-of-life components through single point incremental forming. Manuf Lett 2020;24:132–5. https://doi.org/https://doi.org/10.1016/j.mfglet.2020.05.001.

[14] Piccininni A, Fulco E, Cusanno A, Guglielmi P, Sorgente D, Palumbo G. Gas forming of a deep drawn component for reshaping purposes. Materials Research Proceedings 2025;54:2485–93. https://doi.org/10.21741/9781644903599-268.

[15] Domitner J, Silvayeh Z, Shafiee Sabet A, Öksüz KI, Pelcastre L, Hardell J. Characterization of wear and friction between tool steel and aluminum alloys in sheet forming at room temperature. J Manuf Process 2021;64:774–84. https://doi.org/10.1016/j.jmapro.2021.02.007.

[16] Buffa G, Gucciardi M, Fratini L, Micari F. Multi-directional vs. mono-directional multi-step strategies for single point incremental forming of non-axisymmetric components. J Manuf Process 2020;55:22–30. https://doi.org/10.1016/j.jmapro.2020.03.055.